Original Article

Proteomic landscape of lung adenocarcinoma precancerous lesions reveals mitochondrial dsRNA-associated immune and stress responses

Xizhen Xu^{1,3}, Tianqi Gong², Zitian Huo³, Yaqi Duan³, Qian Chu¹, Jun Qin⁴

¹Department of Oncology, Tongji Hospital, Tongji Medical College, Huazhong University of Science and Technology, Wuhan 430030, Hubei, China; ²Institutes of Biomedical Sciences, Fudan University, Shanghai 200032, China; ³Institute of Pathology, Tongji Hospital, Tongji Medical College, Huazhong University of Science and Technology, Wuhan 430030, Hubei, China; ⁴State Key Laboratory of Proteomics, Beijing Proteome Research Center, National Center for Protein Sciences (Beijing), Beijing Institute of Lifeomics, Beijing 102206, China

Received July 16, 2025; Accepted September 4, 2025; Epub September 15, 2025; Published September 30, 2025

Abstract: Lung adenocarcinoma (LUAD) develops through a stepwise progression from pre-cancerous lesions, including atypical adenomatous hyperplasia (AAH), adenocarcinoma in situ (AIS), and minimally invasive adenocarcinoma (MIA). Understanding the molecular dynamics underlying these transitions is critical for early detection and therapeutic interventions. A comprehensive proteomic analysis was performed on pre-cancerous and early LUAD samples using label-free quantitative mass spectrometry. Immunohistochemistry (IHC) and double fluorescence staining were applied to validate protein expression and mt-dsRNA localization. Trajectory inference was utilized to model dynamic proteomic changes during lesion progression. Mt-dsRNA levels were significantly elevated in pre-cancerous lesions, peaking in AlS. Double fluorescence staining revealed partial co-localization with the mitochondrial marker TOMM20, suggesting mitochondrial origin. Differential γ-H2AX staining patterns, with nuclear positivity in AAH and cytoplasmic positivity in AIS and MIA, indicated stage-specific dynamics of the DNA damage response. Upregulation of dsRNA sensors, including RIG-I and MDA5, and dsRNA-binding proteins (dsRBPs) such as ADAR1 and HNRNPA2/B1, highlighted a complex regulatory feedback network for both oncogenic and antitumorigenic effects. Notably, in dsRNA-IP assay, ASPH was enriched across all stages including LUAD, while TMED9 and HNRNPA2/B1 were specific to pre-cancerous lesions, reflecting their stage-dependent roles in tumor transformation. Finally, Trajectory analysis identified distinct proteomic shifts, with AAH lesions exhibiting high progression scores resembling AIS and MIA, underscoring their malignant potential. This study reveals the multifaceted roles of mt-dsRNA and its associated proteins in pre-cancerous lesions, providing insights into immune activation, stress adaptation, and early carcinogenesis. These findings establish a framework for developing biomarkers and targeted therapies aimed at preventing the transition to invasive LUAD.

Keywords: Lung adenocarcinoma, atypical adenomatous hyperplasia, adenocarcinoma in situ, minimally invasive adenocarcinoma, mitochondrial double-stranded RNA, proteomics

Introduction

Lung adenocarcinoma (LUAD), the most common histological subtype of non-small cell lung cancer (NSCLC), constitutes more than 40% of global lung cancer cases. Although significant progress has been made in therapeutic approaches, including surgical resection, chemotherapy, and immunotherapy, the prognosis for advanced-stage LUAD remains unfavorable, with a five-year survival rate below 20% [1]. This poor survival outcome underscores the critical

importance of early detection and timely therapeutic intervention, which are essential for enhancing patient survival. Therefore, investigating the early pathological mechanisms and progression of LUAD has become a pivotal focus in current oncological research.

Lung adenocarcinoma (LUAD) arises through a well-defined sequence of histopathological and molecular alterations, beginning with preneoplastic lesions. The stepwise progression encompasses atypical adenomatous hyperplasia (AAH), adenocarcinoma in situ (AIS), and minimally invasive adenocarcinoma (MIA), which collectively represent the precursor continuum preceding invasive LUAD [2]. Each of these premalignant stages exhibits distinct histomorphological characteristics and carries a differential risk of malignant transformation.

Atypical adenomatous hyperplasia (AAH), the earliest identifiable preneoplastic lesion, is characterized by small (<5 mm), focal proliferations of mildly dysplastic type II pneumocytes or bronchiolar Clara cells. Regarded as a lowrisk precursor, AAH demonstrates minimal malignant potential. In contrast, adenocarcinoma in situ (AIS) consists exclusively of neoplastic cells exhibiting a lepidic growth pattern along alveolar septa, lacking stromal, vascular, or pleural invasion. Although larger (≤3 cm) than AAH, AIS remains noninvasive yet carries a substantially higher risk of progression to invasive LUAD. Minimally invasive adenocarcinoma (MIA), also ≤3 cm, retains a predominantly lepidic architecture but features focal stromal invasion (≤5 mm)2. This invasive component distinguishes MIA from AIS and confers an elevated risk of aggressive transformation. Precise discrimination among these entities is critical for diagnostic accuracy, prognostic stratification, and clinical management, as early intervention in AIS and MIA significantly improves survival outcomes.

The malignant progression from atypical adenomatous hyperplasia (AAH) to adenocarcinoma in situ (AIS), minimally invasive adenocarcinoma (MIA), and ultimately invasive LUAD is orchestrated by dynamic interplay among somatic mutations, epigenetic dysregulation, and tumor microenvironment (TME) remodeling. Early clonal events in LUAD pathogenesis predominantly involve driver mutations in EGFR, ERBB2, NRAS, and BRAF [3], whereas late-stage progression is marked by TP53 inactivation and aberrations in cell motility-, gap junction-, and metastasis-related genes, reflecting subclonal diversification and malignant evolution. Metabolic dysregulation, particularly disrupted bile acid metabolism, arises during the premalignant phase and actively fuels tumor growth and invasion [4]. Additionally, single-cell RNA sequencing reveals that early neoplastic cells closely resemble alveolar type 2 (AT2) cells but undergo dedifferentiation into a stem-like progenitor state, which drives tumor initiation and sustains progression [5].

Mitochondrial double-stranded RNA (mt-dsR-NA) is a class of nucleic acids generated via bidirectional transcription of mitochondrial DNA (mtDNA), yielding complementary transcripts that form stable double-stranded structures. Under physiological conditions, mt-dsR-NA is rapidly degraded by mitochondrial RNA helicases (e.g., SUV3, PNPase) and associated surveillance machinery, preventing its aberrant accumulation. However, upon mitochondrial membrane leakage or defective RNA quality control, mt-dsRNA can translocate to the cytosol or extracellular space, where it functions as a potent pathogen-associated molecular pattern (PAMP) [6]. The immunogenicity of mt-dsR-NA is mediated through its recognition by cytosolic pattern recognition receptors (PRRs), particularly RIG-I (DDX58) and MDA5 (IFIH1), which initiate downstream signaling cascades via the mitochondrial antiviral signaling protein (MAVS). This interaction triggers the activation of interferon regulatory factors (IRFs) and NF-κB, culminating in the robust production of type I interferons (IFN- α/β) and pro-inflammatory cytokines [7].

Although mt-dsRNA has been implicated in various pathological conditions, including cancer, autoimmunity, and chronic inflammatory diseases, its role in pre-cancerous lung lesions remains poorly understood. Questions surrounding its origin, regulation, and impact on disease progression remain unanswered. In this study, we investigated the proteomics land-scape of pre-cancerous lesions in LUAD and unveiled the multifunctional roles of mt-dsRNA in driving the transition toward invasive LUAD.

Materials and methods

Sample collection

This study was approved by the ethics committee of Tongji Hospital, Tongji Medical College, Huazhong University of Science and Technology. Tumors (diagnosed between from 2019 to 2023) were obtained with informed consent from archival sources at Tongji Hospital, Tongji Medical College, Huazhong University of Science and Technology. The samples were collected from patients at initial diagnosis. All diagnoses were independently reviewed by

three experienced pathologists, and complied with the latest World Health Organization classification standards. The tumors came from patients not treated with neoadjuvant chemotherapy or radiotherapy before operation, with no previous history of malignancy, and diagnosed at the time of surgical resection. All cases were staged according to the National Comprehensive Cancer Network (NCCN) clinical practice guidelines in oncology for small cell lung cancer (version 4.2020).

Immunohistochemistry and assessment

Immunohistochemical staining was conducted using tissue arrays. Prior to de-paraffinization, the slides were heated to 60°C for ten minutes to melt the paraffin. The slides were then washed three times with xylene to solubilize and remove the paraffin. Next, the xylene was removed by washing three times with 100% ethanol followed by 75%, 50% ethanol, and PBS. After the sections were deparaffinized and hydrated, the endogenous peroxidase activity was blocked. Antigen retrieval was performed using the Dako Target Retrieval Solution, High pH (Dako Ominis, Agilent Technologies, CA, USA), in a PTLink set at 98°C for 25 min. The slides were then incubated with the primary antibody at 4°C overnight.

Primary antibodies used in this study were listed in <u>Supplementary Table 1</u>.

Following secondary antibody incubation (~1 hour), the sections were visualized with the DAB kit (ZLI-9017, Zhongshan Biotechnology, Beijing, China) and counterstained with hematoxylin. The stained samples were scored by three pathologists independently for the multiplication of staining intensity (1 - weak; 2 - moderate: 3 - strong) and the percentage of positive tumor cells, which resulted in scores of 0-300. A score of <10 was designated as 0, 10-40 as 1+, 41-140 as 2+, and 141-300 as 3+. All samples with scores of >10 were considered positive cases. For Immunofluorescence, primary and secondary antibodies were incubated similarly as above, followed by DAPI staining. Images were captured using a fluorescence microscope.

Protein extraction, trypsin digestion, and LC-MS/MS processing

For each sample, proteins were extracted from three tissue slices (5- μ m thick) from the FFPE

block (2-5 mm in diameter). The de-paraffinization procedure was the same as IHC as described above. Air dried sample was scraped from the slide and resolubilized in 100 ml of 50 mM NH4HCO3. The sample was then incubated at 95°C for 5 min for de-crosslinking, and cooled to room temperature. Trypsin digestion was carried out at 37°C overnight. Peptides were extracted twice with 200 ul of extraction buffer (50% acetonitrile and 0.1% formic acid in water) with 15 min vortex. The resulting peptides were dried and stored at -80°C for future analysis. The digested peptides were eluted, divided into three fractions, and analyzed on a Q Exactive HF-X or Orbitrap Exploris™ 480 mass spectrometer coupled with an Ultimate 3000 RSLCnano LC system (Thermo Fisher Scientific) and operated at data-dependent acquisition mode. MS1 was measured in the Orbitrap at a resolution of 60,000 followed by tandem MS scans of the top 40 precursors using higher-energy collision dissociation with 27% of normalized collision energy and 15 s of dynamic exclusion time.

Mass spectrometry data analysis

MS Raw files were searched against the National Center for Biotechnology Information (NCBI) Ref-seq human proteome database (updated on 04/07/2013, 27,414 entries) in Firmiana [8], a one-stop proteomic cloud platform for data processing and analysis, implemented with Mascot search engine with Percolator (Matrix Science, version 2.3.01). The following search parameters were used: (1) Mass tolerances were 20 ppm for precursor ions and 0.05 Da for product-ions; (2) Up to two missed cleavages were allowed; (3) The minimal peptide length was seven amino acids; (4) Cysteine carbamidomethylation was set as a fixed modification, and N-acetylation and methionine oxidation were considered variable modifications; and (5) The charges of precursor ions were limited to +2, +3, +4, +5, and +6. The peptide and protein FDR were both set to 1%. A label-free, intensity-based absolute quantification (iBAQ) algorithm was used for protein quantification. The iBAQ values were calculated by dividing the raw intensities by the number of theoretical observable peptides. FOT (fraction of total), calculated by dividing a protein's iBAQ by the sum of iBAOs of all identified proteins in a single experiment, was used as normalized abundance to compare protein abundance across all experiments. The missing value was imputed with 1/10 of the global non-zero minimum value of the sample [9].

dsRNA-IP and dsRNA-seq experiments

We performed dsRNA-IP and dsRNA-seg experiments using intraoperative frozen specimens of pre-neoplastic lung lesions or lung adenocarcinoma. After obtaining the dsRNA-IP samples, mass spectrometry analysis was conducted as previously described. For the RIP RNA samples, strand-specific library construction was performed, followed by quality control using the Bioptic Osep100 system. Highthroughput sequencing was then carried out on the Illumina platform (NovaSeg 6000) with PE150 sequencing. After acquiring the raw sequencing data (Raw Data), the initial step involved data filtering to remove adapter sequences, followed by sequencing quality assessment to obtain high-quality data (Clean Data). The Clean Data were then aligned to the reference genome, followed by quantitative analysis and differential expression analysis.

Bioinformatic analysis

For PCA analysis, we utilized the stats R package (version 3.6.0). Specifically, we first normalized the expression profiles using z-score transformation, followed by dimensionality reduction analysis with the prcomp function to obtain the reduced-dimension matrix. Metascape analysis was conducted online (https://metascape.org) for functional pathway analysis. The on-line tool (Sangerbox tools, http://www.sangerbox.com/tool) was used for generating the plots and heatmap. All other statistical analyses were carried out with R 3.6.1.

Pseudotime-based trajectory inference approach

To estimate the trajectory of pre-cancerous lesions in lung adenocarcinomas, the top 15% of proteins exhibiting the most expression variation across samples were selected from the proteome profiling dataset. The samples were then inferred using the R package SCORPIUS, with the resulting inferred scores designated as PS scores. The estimation of the differentiation potency of samples named were inferred using the R package SCENT. Consensus clustering was performed using the R package ConsensusClusterPlus.

Results

Proteomic dynamics across premalignant lung lesion progression

This study enrolled 10 AAH, 19 AIS, 25 MIA, and 20 LUAD (TNM stage I) samples along with their paired adjacent normal lung tissues (Figure 1A, 1B). The clinical characteristics of these patients were summarized in Supplementary Table 2. We carried out a proteomic study using these samples by label-free quantitative mass spectrometry (MS) (Figure 1C). The protein identities and relative abundances of each case, designated as fraction of total (FOT), are provided in Supplementary Table 3. The PCA plot reveals a clear separation between preinvasive lesions (AAH, AIS, MIA) and their adjacent normal tissues (paraAAH, paraAIS, paraMIA), particularly along PC1, which accounts for 26.53% of the variance. Among the lesions, MIA displays the most distinct proteomic profile, while AAH and AIS cluster more closely together (Figure 1C).

Comparative proteomic analysis of atypical adenomatous hyperplasia (AAH) versus adjacent normal lung tissues demonstrated a predominant downregulation of characteristic proteins, with 133 proteins showing >50% reduction (Figure 1D). Metascape enrichment analysis identified these differentially expressed proteins as functionally clustered in critical structural and microenvironmental pathways: intermediate filament organization, cytoskeletal dynamics in muscle cells, NABA CORE MATRISOME components, hemostasis-related pathways, and extracellular matrix (ECM) organization. The coordinated downregulation of intermediate filament networks likely destabilizes epithelial cell polarity and cell-cell adhesion, initiating dysplastic morphological alterations. Concurrent impairment of muscle cell cytoskeletal components may compromise bronchiolar/alveolar contractility and structural integrity, fostering aberrant proliferative niches. Notably, the depletion of matrisome proteins and ECM remodeling pathways reflects disrupted deposition of collagenous scaffolds and laminin-rich basement membranes - key determinants of tissue biomechanical properties. Such ECM dyshomeostasis perturbs integrin-mediated mechanotransduction, growth factor sequestration, and tissue stiffness gra-

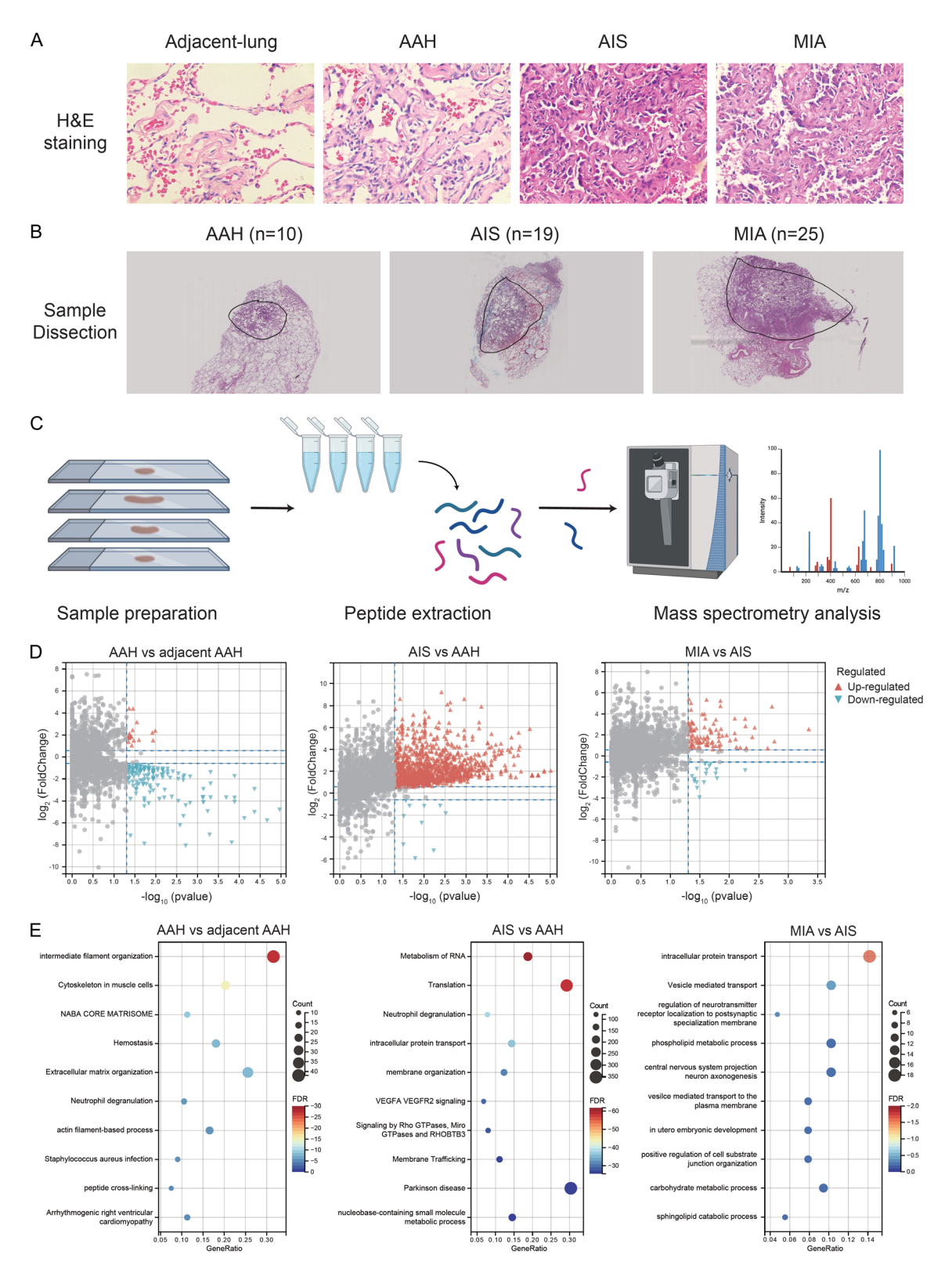


Figure 1. Proteomic dynamics across premalignant lung lesion progression. A. Pathological diagnoses were confirmed and included in the study based on the typical morphological features of HE staining in normal lung, AAH, AIS, and MIA. B. Through comparative section analysis, we selected the lesioned areas for microdissection and sample preparation. C. PCA plot showing separation between preinvasive lesions (AAH, AIS, MIA) and normal tissues (para-AAH, paraAIS, paraMIA). MIA exhibits the most distinct proteomic profile. D. The volcano plot illustrates differentially

DsRNA-induced proteomic changes in lung precancerous lesions

expressed proteins across three comparative groups: AAH versus paracancerous lung tissue, AIS versus AAH, and MIA versus AIS. It reveals three key features: AAH predominantly exhibits down-regulated proteins relative to normal tissue; The transition to AIS demonstrates increased up-regulated proteins mostly; Subsequent MIA progression shows decreasing differential protein expression compared to AIS. E. Metascape enrichment analysis of differently expressed proteins across three comparative groups: AAH versus paracancerous lung tissue, AIS versus AAH, and MIA versus AIS.

dients, collectively generating a permissive microenvironment for premalignant clone expansion. Furthermore, dysregulated hemostasis pathways - marked by altered fibrinogen processing and platelet activation crosstalk - may potentiate localized fibrin deposition and chronic inflammation. These processes are mechanistically linked to early carcinogenic events, including genomic instability via reactive oxygen species and epithelial-mesenchymal transition (EMT) activation through TGF- β signaling (Figure 1E).

In addition, proteomics revealed 1,163 proteins upregulated >2-fold in adenocarcinoma in situ (AIS) versus atypical adenomatous hyperplasia (AAH), with functional enrichment in RNA metabolism, translation, neutrophil degranulation, intracellular trafficking, membrane dynamics, VEGFA-VEGFR2 signaling, and Rho/Miro GTPase pathways (Figure 1D, 1E). These coordinated alterations drive malignant transformation through proliferative amplification, metabolic reprogramming, and microenvironmental crosstalk. The marked upregulation of RNA processing machinery and translation-related proteins underscores a global shift toward oncoprotein biogenesis, fueling unchecked cell cycle progression. Concurrently, neutrophil degranulation signatures - characterized by elevated myeloperoxidase (MPO) and matrix metalloproteinases (MMPs) - induce chronic inflammation and extracellular matrix (ECM) degradation. This inflammatory milieu facilitates immune evasion via PD-L1 upregulation while promoting angiogenic sprouting through VEGF-A secretion. Enhanced intracellular transport systems, including COPII vesicle trafficking and lysosomal exocytosis, enable efficient secretion of growth factors and autocrine receptor recycling, sustaining proliferative signaling. Membrane reorganization processes, such as lipid raft assembly, optimize spatial coordination of VEGFA-VEGFR2 complexes, amplifying angiogenesis to support expanding lesions. Rho GTPases restructure actin networks to enhance motility, while Miro GTPases (MIRO1/2) mediate mitochondrial redistribution along microtubules, coupling energy production to invasion fronts. Paradoxically, RHOBTB3 - a substrate-recognition component of Cullin-3 ubiquitin ligase complexes - exhibits dysregulated expression, potentially compromising its tumor-suppressive role in cell cycle checkpoint control and apoptosis.

Finally, Proteomic profiling identified 127 proteins upregulated >2-fold in minimally invasive adenocarcinoma (MIA) versus adenocarcinoma in situ (AIS), with functional enrichment in intracellular/vesicle-mediated transport, neurotransmitter receptor trafficking, and phospholipid metabolism (Figure 1D, 1E). These adaptive mechanisms collectively orchestrate stromal invasion through secretory reprogramming, membrane plasticity, and metabolic symbiosis. Enhanced intracellular transport machinery, including Rab GTPase-driven vesicular trafficking and COP9 signalosome-mediated exosome biogenesis, facilitates the secretion of matrix-degrading enzymes and pro-invasive cytokines, enabling basement membrane breaching and stromal infiltration. Parallel upregulation of synaptic-like neurotransmitter receptor trafficking pathways - notably glutamate receptor (mGluR) endocytosis and GABAergic receptor recycling - suggests cooption of neuronal regulatory modules. This may potentiate integrin β1/FAK complex redistribution and growth factor receptor clustering at invadopodia, enhancing mechanosensory responses to extracellular stiffness gradients. Phospholipid metabolic rewiring, marked by elevated phospholipase D (PLD) and lysophosphatidic acid (LPA) synthase activity, generates second messengers that activate RHO/ROCKmediated cytoskeletal contractility and PI3K/ AKT survival signaling. Simultaneously, phospholipid enrichment in secretory vesicles promotes membrane curvature generation, facilitating exosome release to precondition the metastatic niche.

The observed pattern - predominant protein downregulation in normal-to-AAH transition, massive upregulation from AAH to AIS, and lim-

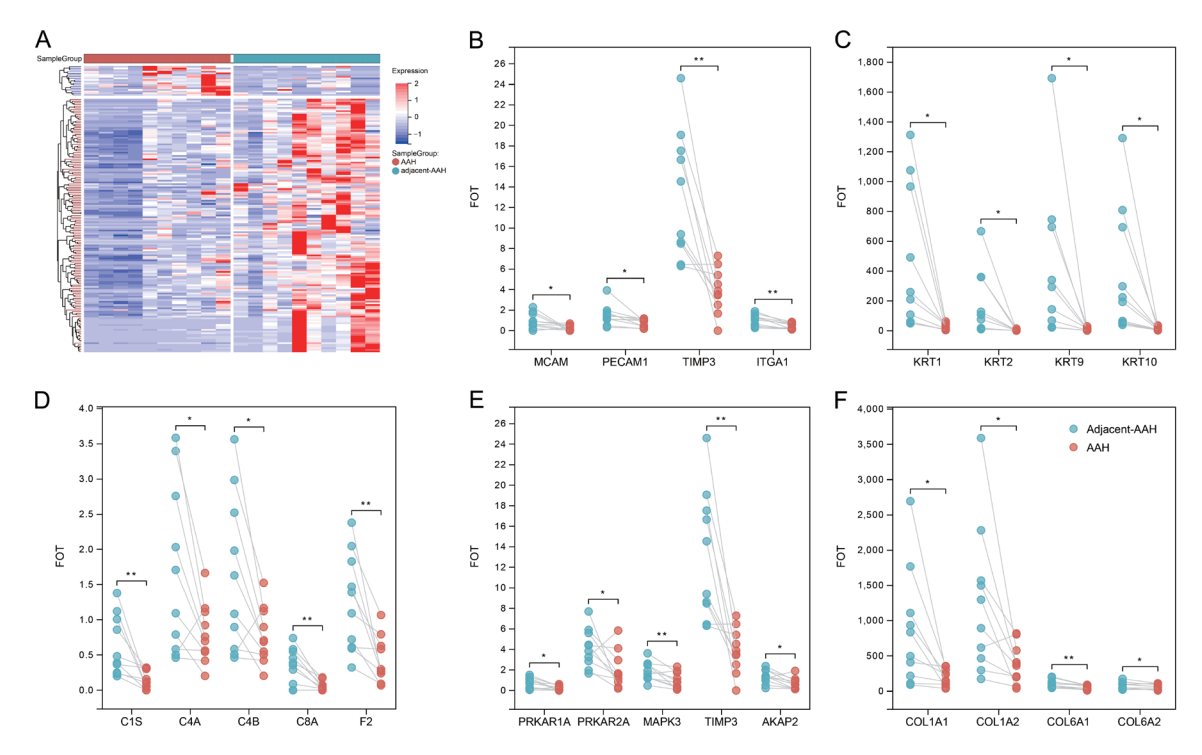


Figure 2. Loss of adhesion and stress response in AAH. (A) Heatmap of downregulated adhesion-related proteins in AAH. (B-F) Paired dot plots depict expression profiles of adhesion regulators (B), Keratins (C), matrix proteins (D), MAPK signaling pathway-related proteins (E), and collagens (F) across sample pairs.

ited upregulation from AIS to MIA - reflects distinct biological shifts during carcinogenesis. Early-stage downregulation (normal→AAH) likely disrupts tissue architecture and homeostasis (e.g., ECM, cytoskeleton), enabling dysplastic initiation. The subsequent surge in protein expression (AAH - AIS) marks aggressive activation of proliferation (translation, metabolism), inflammatory signaling (neutrophil degranulation), and angiogenesis (VEGFA-VEGFR2), driving premalignant expansion. Finally, the modest upregulation (AIS→MIA) suggests a shift toward microenvironmental adaptation (vesicle transport, phospholipid metabolism) and invasive specialization, prioritizing cellular motility and stromal remodeling over bulk growth. This dynamic progression highlights stage-specific vulnerabilities for targeted interventions.

Proteomics revealed AAH was characterized by loss of adhesion, early infiltration of macrophages, and cellular response to stress

In the AAH stage, loss of adhesion was one of the most significant characteristics (**Figure 2A**). The most obviously decreased proteins included matrix proteins such as C1S, C4A,

C4B, C8A, F2, collagens such as COL1A1, COL1A2, COL6A1, COL6A2, Keratins such as KRT1/2/9/10, and adhesion regulators such as MCAM, PECAM1, TIMP3, and ITGA1. Meanwhile, MAPK3, AKAP2, PALM2, PRKAR1A, and PRKAR2A were also decreased compared with adjacent lung tissues, indicating an inhibition of MAPK signal pathway (Figure 2B-F). However, this inhibition of MAPK was transient in AAH as it was not detected in later stages of AAH and MIA.

Of the up-regulated proteins in AAH, the expression of macrophage specific markers MRC1(CD206) and ALOX5 were significant (Figure 3A). To validate the immune infiltration status in pre-cancerous lesions of lung adenocarcinoma, we conducted immunohistochemistry of CD4, CD8, and CD163. As a result, significant infiltration of CD163 positive macrophages were observed in AAH (Figure 3B) while it was not obvious for CD4 or CD8 positive T cells (data not shown). What's more, metascape analysis suggested the overexpressed proteins in AAH were enriched in the regulation of cellular response to stress (especially the response to endoplasmic reticulum stress), mainly including ALOX5, UBQLN1, DDRGK1 (Figure 3C).

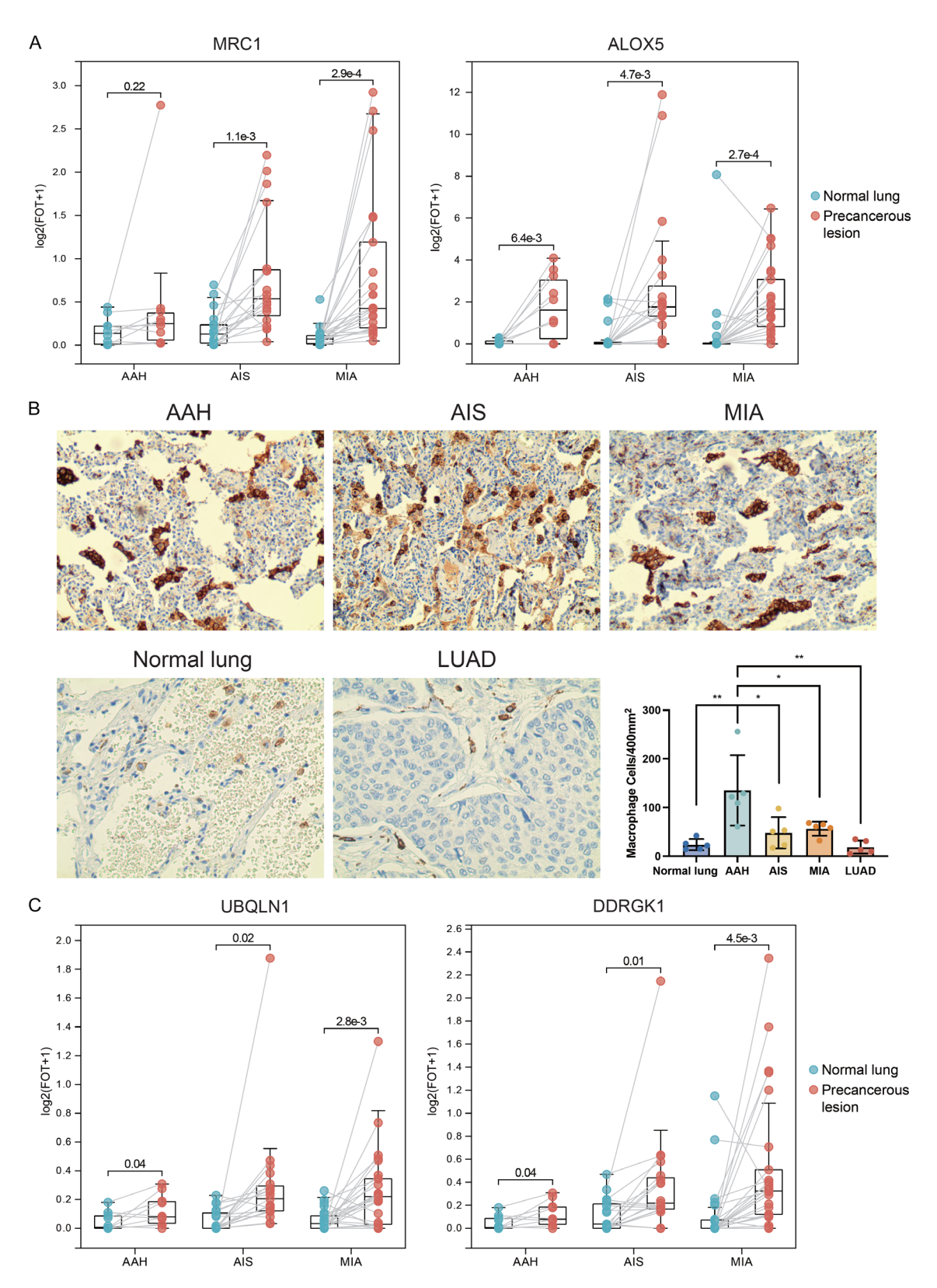


Figure 3. Immune infiltration and cellular stress in AAH. A. Upregulated macrophage markers (MRC1/CD206, ALOX5) in AAH. B. IHC validation of CD163+ macrophage infiltration in AAH. C. Paired dot plots depict expression profiles of stress-response proteins in AAH, linked to endoplasmic reticulum stress.

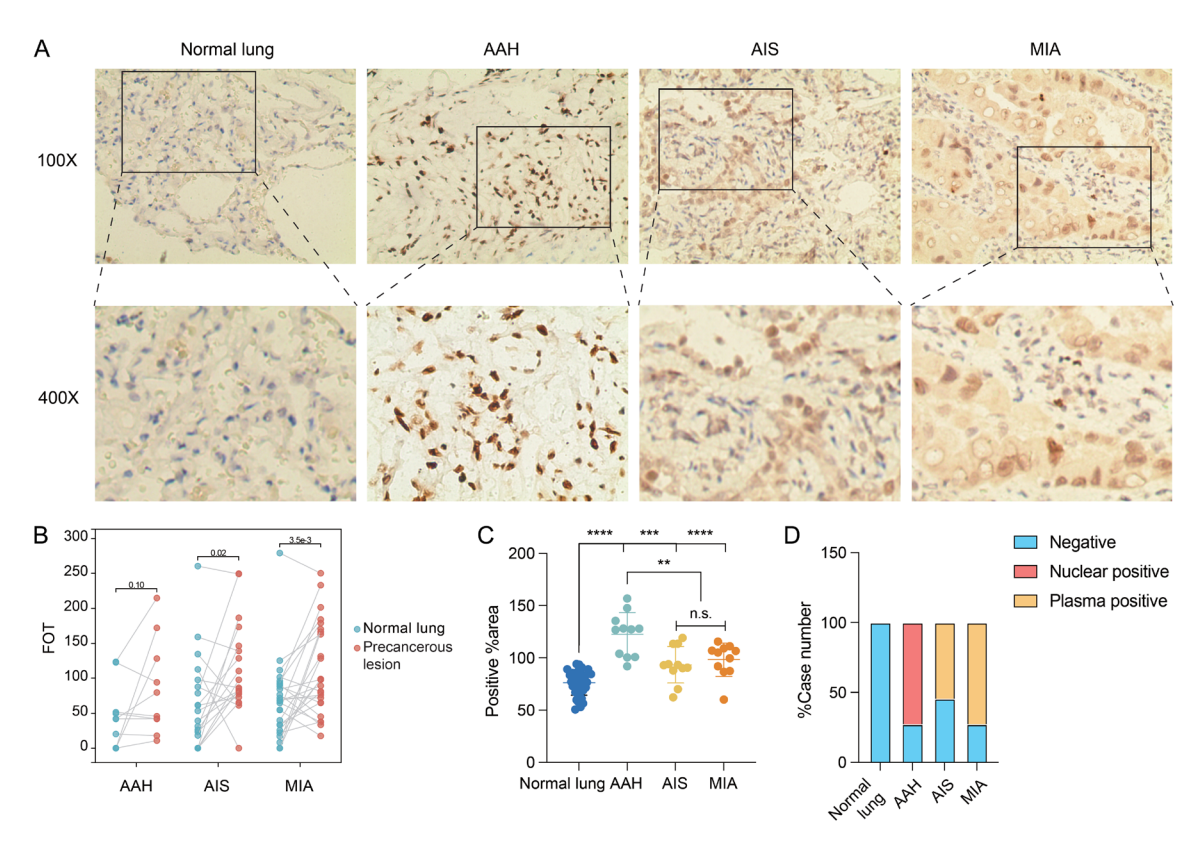


Figure 4. DNA Damage Response in Premalignant Lesions. A. IHC staining of γ -H2AX (DNA damage marker) in AAH (nuclear positivity) vs. AIS/MIA (cytoplasmic positivity). B. Proteomic data showing H2AFX upregulation in premalignant stages. C, D. Quantification of γ -H2AX staining patterns across stages, reflecting stage-specific DNA damage dynamics.

DNA damage and response occurred in precancerous lesions of lung adenocarcinoma

Considering the growing stress in precancerous lesions, we observed that H2AFX was also upregulated (Figure 4B). One of the earliest events in response to nascent DNA damage in human cells is the phosphorylation of the histone variant H2AX on serine 139, forming y-H2AX, a sensitive marker for DNA doublestrand breaks (DSBs) [10]. To validate the presence of DNA damage, we performed immunohistochemical staining of γ -H2AX (**Figure 4A**). Interestingly, y-H2AX showed predominant nuclear localization in 8 out of 11 AAH cases, while both nuclear and cytoplasmic signals were detected in 6 out of 11 AIS and 8 out of 11 MIA samples (Figure 4C, 4D). Although cytoplasmic y-H2AX staining was observed in AIS and MIA, it remains possible that this may not solely reflect translocation from the nucleus. We cannot exclude the possibility that the cytoplasmic staining results from antibody crossreactivity with unknown antigens upregulated in these lesions. Therefore, this interpretation should be considered with caution.

Expression of dsRNA sensors started increasing in AIS and MIA

Innate immune sensors of dsRNA included the RIG-I-like receptors (RLRs) and dsRNA sensor PKR (encoded by EIF2AK2). RLRs are represented by three proteins: RIG-I, MDA5, and LGP2 (encoded by DDX58, IFIH1, and DHX58, respectively) (Figure 5A, 5B). Binding of either RIG-I or MDA5 to dsRNA drives induction of IFN signaling through activation of MAVS. Here in our study, DDX58, IFIH1, and MAVS were detected to be up-regulated in AIS and MIA rather than AAH, instigating a further IFN response. On the other hand, protein kinase R (PKR) and oligoadenylate synthases (OASs) induce growth inhibition by disrupting protein synthesis and degrading RNA. Unlike the RIG-I family members, the dsRNA sensor PKR (encoded by EIF2AK2) binds to dsRNA via two dsRNA-binding domains. The primary substrate

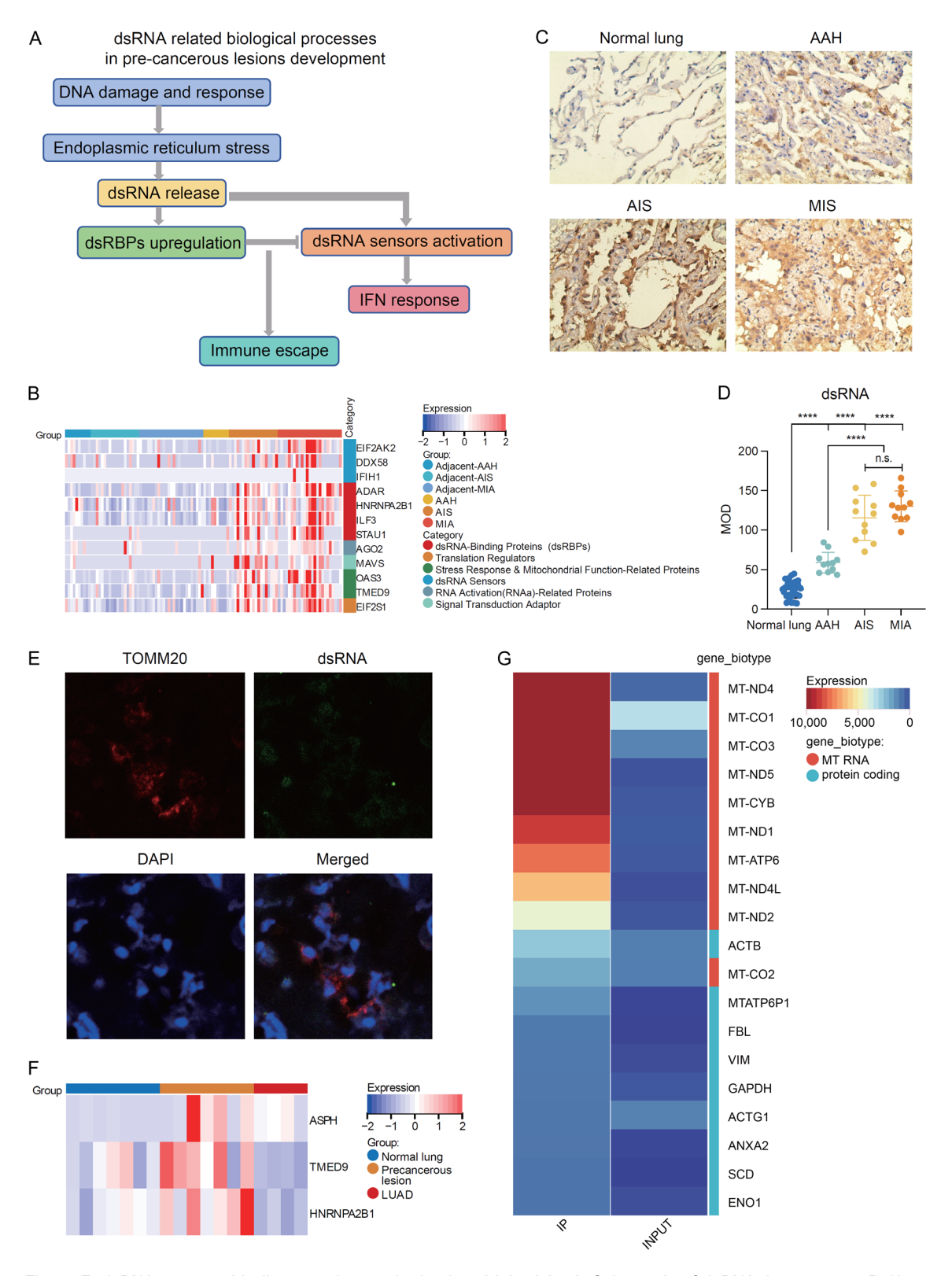


Figure 5. dsRNA sensors, binding proteins, and mitochondrial origin. A. Schematic of dsRNA downstream. B. Heatmap of upregulated dsRNA-related protein. C. IHC with J2 antibody showing dsRNA accumulation in AAH-AIS-MIA (peak in AIS). D. Quantification of dsRNA levels across stages. E. Co-IF staining of dsRNA and TOMM20, confirming mitochondrial origin. F. dsRNA-IP assay identifying stage-specific binders. G. RIP-seq of mitochondrial dsRNA in premalignant lesions.

of PKR is the translation initiation factor eIF2a (encoded by EIF2S1). Interestingly, EIF2AK2, EIF2S1, and OAS3 also started increasing in AIS and MIA, indicating a function of barrier in carcinogenesis (**Figure 5B**).

dsRNA-binding proteins (dsRBPs) was up-regulated along with dsRNA sensors in AIS and MIA

Mammals have three ADARs, each with a C-terminal catalytic domain and 2 or 3 dsRBDs [11]. The adenosine to inosine (A-to-I) editing by ADAR1 within dsRNA is essential for marking "self" RNAs and suppressing activation of dsRNA sensors. ADAR1 has two isoforms, p150 and p110, and it is p150 that is responsible for suppression of dsRNA sensing by MDA5 and PKR. The two isoforms are generated through the use of two promoters, and although the longer isoform is canonically thought of as being IFN inducible, both isoforms are induced to some extent by IFN signaling. The human ADAR2 protein is encoded by the gene ADARB1. The editing function of ADAR2 is essential in mice where it edits the GRIA2 mRNA, which encodes an AMPA (a-amino-3-hydroxy-5-methyl-4-isoxazole propionate) glutamate receptor. Editing of GRIA2 mRNA converts a CAG codon to CIG, thus recoding the mRNA to make Arg in place of Gln in the protein product. Notably, in our study only ADAR1 rather than ADAR2 was up-regulated in AIS and MIA. In humans, the ADAR3 protein is encoded by the gene ADARB2. ADAR3 has no catalytic activity and has the ability to bind single-stranded RNA. But ADAR3 was not detected in our study.

What's more, the STAU1 and NF90 (encoded by ILF3) were increased in AIS and MIA. STAU1 binding is important to overcome nuclear retention for dsRNA. NF90 stabilizes the mRNAs by competing with the dsRBPs STAU1 for binding, thus preventing SMD of pro-mitotic mRNAs [12, 13]. Although overexpression of the dsRBDs of ADAR1, ADAR2, or STAU1 each could prevent activation of PKR in the absence of ADAR1, ADAR1 also inhibits STAU1 function in an editing-independent way, by competing for its dsR-NA-binding sites. That is to say there existed a complex competition between STAU1, ADAR1, and PKR. And the up-regulation of dsRBPs might be a negative feedback towards dsRNA activated IFN signalling.

The rising dsRNA in pre-cancerous lesions was validated by IHC and co-IF

According to previous reports, mt-dsRNA foci are almost not detected in slow-dividing and quiescent cell cultures, however, upon in vitro model of malignant transformation with telomerase reverse transcriptase (hTERT), the large T antigen of simian vacuolating virus 40 (LT) oncoprotein and the oncogenic RAS allele. HRAS^{G12V}, the fully carcinogenic cell line, hTERT-LT-RAS, readily formed colonies and exhibited higher oxygen consumption rates and extracellular acidification rates. Meanwhile, mt-dsRNA foci were only detected upon additional expression of SV40LT and further increased in number and intensity after the expression of HRAS^{G12V} [14]. In addition, it was also reported that mt-dsRNA was accumulated in human lung adenocarcinoma.

Firstly, through immunohistochemical detection with the J2 monoclonal antibody (**Figure 5C**), we verified that dsRNA started increasing in AAH compared with adjacent lung tissues, which was earlier than the protein expression change of dsRNA sensors or binding proteins. The rising of dsRNA seemed transient during the pre-cancerous stages of lung adenocarcinoma. The positive staining was most obvious in AIS, gradually lower in MIA (**Figure 5D**). In addition, double fluorescence staining of dsRNA and TOMM20 found dsRNA was partly co-located with TOMM20, suggesting the rising dsRNA may come from mitochondrion (**Figure 5E**).

Identification of dsRNA-binding proteins and sequencing of dsRNA

Compared with lung, the dsRNA-IP assay (Supplementary Table 4) identified three possible dsRBPs which had special function in precancerous progression of lung adenocarcinoma, including ASPH, TMED9, and HNRNPA2B1 (Figure 5F). Of them, ASPH was highly enriched by dsRNA-pull down assay in both pre-cancerous lesions and LUAD while both TMED9 and HNRNPA2B1 were only highly detected in precancerous lesions rather than LUAD samples. What's more, all of these three proteins were not significantly up-regulated in AAH but increased in AIS/MIA in previous proteomic landscape results.

Small activating dsRNA [double-stranded RNA; saRNA (small activating dsRNA)] complementary to promoter regions can up-regulate gene expression in mammalian cells, a phenomenon termed RNAa (RNA activation) [15]. hnRNPA2/B1 interacts with the saRNA in vivo and in vitro and is required for RNAa activity. Besides, RNAa requires the AGO2 (argonaute 2) protein to regulate RNAi [16]. In our results, the rising expression of AGO2 was significantly obvious in MIA rather than AAH and AIS, which also confirmed RNAa as a downstream effect of hnRN-PA2/B1 and dsRNA binding.

We further conducted a J2 antibody-based dsRNA Immunoprecipitation mass spectrum RIP-seq (Supplementary Table 5). As a result, we identified many dsRNA sequences related with mitochondrial in the pre-cancerous lesions. These sequences included MT-ND4, MT-ND5, MT-ND4L, MT-CYB, MT-ATP6, MT-ND1, MT-ND2, MT-CO3, MT-CO1, MT-ATP8, and PEMT (log2FC >2) (Figure 5G), all of which were involved in the electron transport chain OXPHOS system in mitochondria and oxidative phosphorylation. Moreover, Aminoacyl-tRNA biosynthesis related genes including MT-TT, MT-TE, and MT-TY were also significant. These results indicated that dsRNA was predominantly released from mitochondria, and that mitochondrial stress signals were translocated to the cytosol during the precancerous progression of LUAD.

New risk evaluation model for pre-cancerous lesions based on proteomic data

In this study, we applied a pseudotime-based trajectory inference approach on proteomic expression data derived from pre-cancerous lung lesions (Supplementary Table 6) to provide a dynamic view of how protein expression evolves during the transition from normal to pre-cancerous states. This method allows for the reconstruction of the progressive trend in the proteomic landscape, and revealed a with distinct shifts in protein abundance corresponding to different stages of lesion development.

The inferred trajectories of changes revealed trends similar to those observed in the different stages of lesion development. Specifically, the closer the inferred temporal score is to 1, the more advanced the stage of precancerous pro-

gression. Cancer samples exhibited higher inferred values compared to adjacent normal tissues (Figure 6A). Notably, we found that some AAH samples still displayed relatively high inferred temporal scores. Additionally, we employed consensus clustering and single-cell differentiation potency estimation to evaluate the proteomic changes associated with early lung cancer lesions. Both methods led to similar conclusions, with a strong correlation (r = 0.91) between the PS score and SR score (Figure 6B). The consensus clustering analysis classified the samples into four clusters. Cluster 1 primarily consisted of nearly all LUAD tumor samples, about half of MIA and AIS tumor samples, and a smaller proportion of AAH samples (Figure 6C, 6D). In contrast, Clusters 3 and 4 were largely composed of para-tumor samples. Moreover, we observed that the expression of the aforementioned molecules followed an increasing trend with the inferred trajectory PS score, suggesting their potential role in driving early tumorigenic processes.

Discussion

Mitochondrial double-stranded RNA (mt-dsR-NA) has emerged as a key player in cancer biology, serving both as a mediator of immune responses and as a factor influencing tumor progression. mt-dsRNA is produced from bidirectional transcription of mitochondrial DNA and typically degraded by mitochondrial surveillance mechanisms [17]. However, in cancer, mitochondrial dysfunction often leads to the accumulation and release of mt-dsRNA into the cytoplasm or extracellular space. The escape of mt-dsRNA from mitochondria occurs due to stress-related mitochondrial membrane permeability changes or defective RNA degradation. Here our study uncovered several significant roles of mitochondrial-derived doublestranded RNA (mt-dsRNA) and its associated proteins in pre-cancerous lesions of lung adenocarcinoma (LUAD), emphasizing its mu-Itifaceted involvement in immune activation, cellular stress responses, and early tumor progression.

Proteomic analysis highlighted dynamic changes in protein expression during the transition from AAH to AIS, MIA, and invasive LUAD. Early loss of adhesion-related proteins (e.g., collagens, keratins) was identified in AAH, correlating with tissue remodeling and immune infiltra-

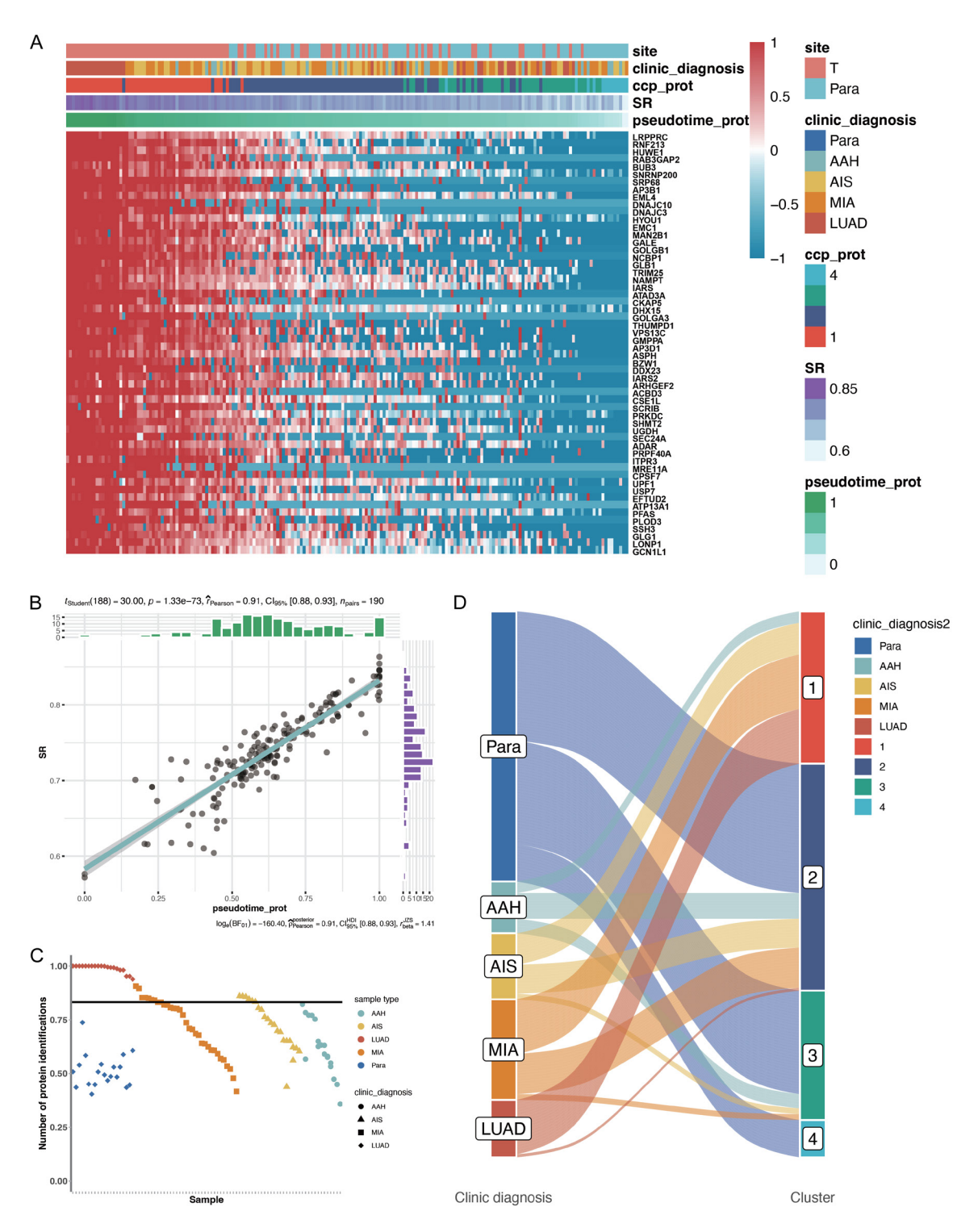


Figure 6. Trajectory analysis of proteomic progression. A. Pseudotime trajectory (SCORPIUS) showing progression scores (PS): higher scores correlate with advanced stages (LUAD>MIA>AIS>AAH). Some AAH samples exhibit high PS, indicating malignant potential. B. Correlation (r = 0.91) between PS scores and single-cell potency scores (SR). C, D. The consensus clustering analysis classified the samples into four clusters. Cluster 1 primarily consisted of nearly all LUAD tumor samples, about half of MIA and AIS tumor samples, and a smaller proportion of AAH samples.

tion. Upregulation of stress-related proteins, such as ALOX5, UBQLN1, and DDRGK1, was

evident in response to endoplasmic reticulum stress in AAH.

Increased expression of y-H2AX, a marker for DNA double-strand breaks (DSBs), was observed in pre-cancerous lesions by both proteomics data and IHC verification. The observation of differential patterns of y-H2AX staining nuclear-positive and cytoplasmic (plasma)-positive - in pre-cancerous lesions suggests distinct underlying biological processes and may provide insights into the stage-specific dynamics of DNA damage response (DDR) and cellular stress in lung adenocarcinoma progression. Nuclear positivity indicates active DDR in response to genotoxic stress, which is common in pre-cancerous lesions as cells experience replication stress or oxidative damage. In AAH, nuclear y-H2AX may reflect an attempt by cells to manage replicative stress and maintain genomic stability, potentially serving as a tumor-suppressive mechanism. Cytoplasmic v-H2AX may result from aberrant phosphorylation of H2AX under conditions of extreme cellular stress or mitochondrial dysfunction, disrupting its normal nuclear localization. Mislocalization could be linked to impaired nuclear-cytoplasmic transport pathways, often altered in tumorigenic processes. Predominantly Nuclear y-H2AX indicated an active DDR attempting to repair DSBs caused by early genomic instability or oxidative stress, and suggested a protective response to prevent malignant transformation. In the advanced Pre-Cancerous Stages (e.g., MIA), predominantly cytoplasmic γ-H2AX suggested impaired DDR and increased mitochondrial distress, contributing to genomic instability.

In addition, Proteomics detected RIG-I (encoded by DDX58) and MDA5 (encoded by IFIH1) were significantly upregulated in AIS and MIA. The dsRNA sensor PKR (encoded by EIF2AK2) and its substrate eIF2α (EIF2S1) were also upregulated. Activation of RIG-I and MDA5 downstream signaling through the MAVS protein led to type I interferon (IFN-I) production and pro-inflammatory cytokine release. This may play an anti-tumorigenic role by inducing immune surveillance mechanisms, recruiting cytotoxic T cells and promoting apoptosis of damaged or pre-cancerous cells. At the same time, dsRNA sensor PKR activation led to growth inhibition and stress adaptation. Chronic activation of PKR may drive adaptive stress responses in tumor cells, enabling survival under adverse conditions such as hypoxia or nutrient deprivation. PKR signaling may also modulate inflammatory pathways (e.g., NF-kB), creating a tumor-promoting microenvironment. On the other hand, dsRNA-Binding Proteins (dsRBPs) activation served as a feedback mechanism to modulate IFN-I responses. ADAR1 (adenosine deaminase acting on dsRNA) was upregulated in AIS and MIA, which performed A-to-I editing of dsRNA to reduce immune activation by masking dsRNA from sensors like MDA5 and PKR. Meanwhile, STAU1 facilitated nuclear export of dsRNA, while NF90 stabilized mRNAs to prevent degradation. What's more, HNRNPA2/B1 interacted with dsRNA to mediate RNA activation (RNAa), promoting transcriptional upregulation of target genes [18]. Increased the expression of oncogenic pathways via RNAa can promote cell proliferation and invasion in pre-cancerous lesions.

The downstream proteins of dsRNA play critical and divergent roles in pre-cancerous lesions, either promoting or suppressing the transition to malignancy. Understanding these roles in the context of tumor microenvironment and stage-specific expression provides a framework for targeted therapies aimed at disrupting pro-tumorigenic signals while reinforcing antitumorigenic defenses. Targeting pro-tumorigenic proteins like ADAR1 and hnRNPA2/B1 can restore immune detection and suppress oncogenic pathways. Enhancing the activity of antitumorigenic proteins like RIG-I and OAS could boost immune responses in pre-cancerous lesions, preventing progression to malignancy. Stage-specific interventions tailored to the dominant dsRNA-related proteins could optimize therapeutic outcomes.

By IHC verification, mt-dsRNA levels were shown to increase significantly in pre-cancerous lesions (AAH, AIS, MIA) compared to adjacent normal lung tissues, with the highest levels observed in AIS. The double fluorescence staining analysis revealed that mt-dsRNA was partially co-localized with the mitochondrial marker TOMM20, suggesting its mitochondrial origin. The dsRNA-pull-down assay identified three critical proteins. ASPH was enriched in both pre-cancerous lesions and invasive LUAD while TMED9 and HNRNPA2/B1 were specific to pre-cancerous lesions. This difference likely reflects stage-specific roles and biological functions of these proteins during the progression

from pre-cancerous stages to invasive cancer. Pre-cancerous lesions experience significant cellular stress (e.g., mitochondrial dysfunction, ER stress) that requires specialized proteins like TMED9 and HNRNPA2/B1 to manage RNA processing and homeostasis. As lesions transition to invasive cancer, the cellular stress response may adapt or shift to pathways that no longer require these proteins, leading to their downregulation.

Finally, the inferred trajectories of changes analysis played a pivotal role in contextualizing and reinforcing the proteomic findings of the study by providing a dynamic and temporal perspective on the progression of pre-cancerous lesions to invasive lung adenocarcinoma (LUAD). This method offers a dynamic and quantitative framework that complements traditional histopathological and molecular analyses, enabling improved diagnostic, prognostic, and therapeutic strategies. The trajectory analysis identified distinct clusters of lesions with varying progression scores, highlighting precancerous lesions with higher malignant potential. AAH samples with higher inferred scores showed proteomic features resembling AIS or MIA, suggesting they represent high-risk lesions requiring closer monitoring or early intervention. What's more, targeting these proteins in high-risk lesions could delay or prevent the transition to invasive LUAD, representing a preventive therapeutic strategy.

In conclusion, while mt-dsRNA accumulation in pre-cancerous lung lesions represents a promising area of investigation, much remains unknown about its regulation, functional consequences, and clinical relevance. Addressing these gaps will require comprehensive profiling and mechanistic studies to uncover the role of mt-dsRNA in early lung carcinogenesis and its potential as a diagnostic or therapeutic target. The downstream proteins of dsRNA play critical and divergent roles in pre-cancerous lesions, either promoting or suppressing the transition to malignancy. Understanding these roles in the context of tumor microenvironment and stage-specific expression provides a framework for targeted therapies aimed at disrupting pro-tumorigenic signals while reinforcing antitumorigenic defenses. Targeting dsRNA pathways offers a versatile approach to modulating immune responses, with the potential to enhance anti-tumor immunity in cancer or suppress hyperactive immune responses in autoimmune diseases. Advances in understanding dsRNA biology and developing selective, context-specific therapies will pave the way for innovative treatments that harness the power of dsRNA signaling for diverse clinical applications. Future research integrating multi-omics approaches and clinical workflows can unlock the full potential of trajectory analyses and proteomics for early detection, risk stratification, and targeted therapies in lung cancer prevention and treatment.

Acknowledgements

We thank the Mass Spectrometry Platform of National Center for Protein Sciences (Beijing) (PHOENIX Center) for technical assistance. We also thank all the patients who participated in this study, as well as the clinicians and staff of the institutions who assisted with the studies. This study was supported by grants from the National Natural Science Foundation of China. No. 82472969 (Qian Chu), 81974016 (Guoping Wang).

The written informed consent was obtained from the participating patients.

Disclosure of conflict of interest

Jun Qin is the cofounders and co-owners of the Beijing Pineal Diagnostics Co., Ltd.

Address correspondence to: Qian Chu, Department of Oncology, Tongji Hospital, Tongji Medical College, Huazhong University of Science and Technology, Wuhan 430030, Hubei, China. E-mail: qianchu@tjh. tjmu.edu.cn; Jun Qin, State Key Laboratory of Proteomics, Beijing Proteome Research Center, National Center for Protein Sciences (Beijing), Beijing Institute of Lifeomics, Beijing 102206, China. E-mail: jqin1965@126.com

References

- [1] Alsatari ES, Smith KR, Galappaththi SPL, Turbat-Herrera EA and Dasgupta S. The current roadmap of lung cancer biology, genomics and racial disparity. Int J Mol Sci 2025; 26: 3818.
- [2] Chen P, Rojas FR, Hu X, Serrano A, Zhu B, Chen H, Hong L, Bandyoyadhyay R, Aminu M, Kalhor N, Lee JJ, El Hussein S, Khoury JD, Pass HI, Moreira AL, Velcheti V, Sterman DH, Fukuoka J, Tabata K, Su D, Ying L, Gibbons DL, Heymach JV, Wistuba II, Fujimoto J, Solis Soto LM, Zhang

- J and Wu J. Pathomic features reveal immune and molecular evolution from lung preneoplasia to invasive adenocarcinoma. Mod Pathol 2023; 36: 100326.
- [3] Zhang J, Zhou W, Li N, Li H, Luo H and Jiang B. Multi-omics analysis unveils immunosuppressive microenvironment in the occurrence and development of multiple pulmonary lung cancers. NPJ Precis Oncol 2024; 8: 155.
- [4] Zhang C, Zhang J, Xu FP, Wang YG, Xie Z, Su J, Dong S, Nie Q, Shao Y, Zhou Q, Yang JJ, Yang XN, Zhang XC, Li Z, Wu YL and Zhong WZ. Genomic landscape and immune microenvironment features of preinvasive and early invasive lung adenocarcinoma. J Thorac Oncol 2019; 14: 1912-1923.
- [5] Hu X, Fujimoto J, Ying L, Fukuoka J, Ashizawa K, Sun W, Reuben A, Chow CW, McGranahan N, Chen R, Hu J, Godoy MC, Tabata K, Kuroda K, Shi L, Li J, Behrens C, Parra ER, Little LD, Gumbs C, Mao X, Song X, Tippen S, Thornton RL, Kadara H, Scheet P, Roarty E, Ostrin EJ, Wang X, Carter BW, Antonoff MB, Zhang J, Vaporciyan AA, Pass H, Swisher SG, Heymach JV, Lee JJ, Wistuba II, Hong WK, Futreal PA, Su D and Zhang J. Multi-region exome sequencing reveals genomic evolution from preneoplasia to lung adenocarcinoma. Nat Commun 2019; 10: 2978.
- [6] Hu J, Chen Z, Xia D, Wu J, Xu H and Ye ZQ. Promoter-associated small double-stranded RNA interacts with heterogeneous nuclear ribonucleoprotein A2/B1 to induce transcriptional activation. Biochem J 2012; 447: 407-416.
- [7] Grochowska J, Czerwinska J, Borowski LS and Szczesny RJ. Mitochondrial RNA, a new trigger of the innate immune system. Wiley Interdiscip Rev RNA 2022; 13: e1690.
- [8] Feng J, Ding C, Qiu N, Ni X, Zhan D, Liu W, Xia X, Li P, Lu B, Zhao Q, Nie P, Song L, Zhou Q, Lai M, Guo G, Zhu W, Ren J, Shi T and Qin J. Firmiana: towards a one-stop proteomic cloud platform for data processing and analysis. Nat Biotechnol 2017; 35: 409-412.
- [9] Huang W, Zhan D, Li Y, Zheng N, Wei X, Bai B, Zhang K, Liu M, Zhao X, Ni X, Xia X, Shi J, Zhang C, Lu Z, Ji J, Wang J, Wang S, Ji G, Li J, Nie Y, Liang W, Wu X, Cui J, Meng Y, Cao F, Shi T, Zhu W, Wang Y, Chen L, Zhao Q, Wang H, Shen L and Qin J. Proteomics provides individualized options of precision medicine for patients with gastric cancer. Sci China Life Sci 2021; 64: 1199-1211.

- [10] Zhang S, Xu X, ZhangK, Lei C, Xu Y, Zhang P, Zhang Y, Gu H, Huang C and Qiu Z. Targeting OAS3 for reversing M2d infiltration and restoring anti-tumor immunity in pancreatic cancer. Cancer Immunol Immunother 2024; 74: 37.
- [11] Rainaldi J, Mali P and Nourreddine S. Emerging clinical applications of ADAR based RNA editing. Stem Cells Transl Med 2025; 14: szaf016.
- [12] Almasi S and Jasmin BJ. The multifunctional RNA-binding protein Staufen1: an emerging regulator of oncogenesis through its various roles in key cellular events. Cell Mol Life Sci 2021; 78: 7145-7160.
- [13] Grasso G and Kiernan R. The polyvalent role of NF90 in RNA biology. Int J Mol Sci 2022; 23: 13584.
- [14] Xavier V, Martinelli S, Corbyn R, Pennie R, Rakovic K, Powley IR, Officer-Jones L, Ruscica V, Galloway A, Carlin LM, Cowling VH, Le Quesne J, Martinou JC and MacVicar T. Mitochondrial double-stranded RNA homeostasis depends on cell-cycle progression. Life Sci Alliance 2024; 7: e202402764.
- [15] Qian Y, Liu C, Zeng X and Li LC. RNAa: mechanisms, therapeutic potential, and clinical progress. Mol Ther Nucleic Acids 2025; 36: 102494.
- [16] Salman Hameed M, Ren Y, Tuda M, Basit A and Urooj N. Role of argonaute proteins in RNAi pathway in Plutella xylostella: a review. Gene 2024; 903: 148195.
- [17] Sadeq S, Al-Hashimi S, Cusack CM and Werner A. Endogenous double-stranded RNA. Noncoding RNA 2021; 7: 15.
- [18] Liu Y and Shi SL. The roles of hnRNP A2/B1 in RNA biology and disease. Wiley Interdiscip Rev RNA 2021; 12: e1612.